JR Harrison et al.

# Progress Toward Divertor Detachment in TCV H-mode Discharges

# Progress Toward Divertor Detachment in TCV H-mode Discharges

J. R. Harrison[1], C. Theiler[2], O. Février[2], H. de Oliviera[2], R. Maurizio[2], K. Verhaegh[2,4], A Perek[4], A. Karpushov[2], B. Lipschultz[3], B. P. Duval[2], X. Feng[6], S. Henderson[1], B. Labit[2], B. Linehan[5], A. Merle[2], H. Reimerdes[2], U. Sheikh[2], C. K. Tsui, W. A. J. Vijvers, C. Wüthrich, and the TCV team[†] and the EUROfusion MST1 team[*]

[1.] CCFE, Culham Science Centre, Abingdon, Oxon, OX14 3DB, United Kingdom

[2.] Ecole Polytechnique Fédérale de Lausanne (EPFL), Swiss Plasma Center (SPC), Lausanne, Switzerland

[3] York Plasma Institute, Department of Physics, University of York, Heslington, York, YO10 5DD, United Kingdom

[4] DIFFER - Dutch Institute for Fundamental Energy Research, De Zaale 20, 5612 AJ Eindhoven, the Netherlands

[5] Plasma Science and Fusion Center MIT, Cambridge, MA, USA, 02139

[6] Centre for Advanced Instrumentation, Durham University, South Road, Durham, DH1 3LE, UK

## Abstract

Recent experiments on TCV have made significant progress toward partial detachment of the outer divertor in neutral beam heated H-mode plasmas. The heating power required to enter H-mode was measured in a range of divertor configurations, finding that, in the vicinity of the minimum of the $P_{L-H}/n_e$ curve, the threshold power is largely independent of the divertor configuration, such as poloidal flux expansion and major radius of the outer divertor, and in the snowflake minus configuration. In ELM-free scenarios, fuelling and nitrogen seeding were used to cool the divertor sufficiently to achieve a factor 2 reduction in the total divertor power load, but no significant reduction in the total divertor particle load was observed. ELM-free scenarios were used to study the impact of outer divertor poloidal flux expansion on divertor cooling, finding that it does not have a significant effect. Experiments in ELMy H-mode plasmas using nitrogen seeding were able to achieve a factor 2 reduction in the outer divertor power load and a ~30% reduction in the particle flux. The influence of outer target major radius in ELMy H-mode experiments studied divertor cooling where the strike point was placed at R = 0.75m and 1.03m, indicating slightly higher amenability to real-time control of the front location.

## 1. Introduction

The reliable operation of future high power density magnetic confinement fusion reactors such as ITER [Shimada2007] and DEMO [Wenninger2014] requires that the power and particles leaving the confined plasma can be exhausted in such a way that avoids the limits of plasma-facing materials in the divertor and first wall. In ITER, this material limit for steady-state power loads is ~10MWm$^{-2}$ [Pitts2017], and lower in DEMO [Wenninger2014]. For example, in a DEMO reactor with a net electric power output of 500MW [Wenninger2014], if the material limit is taken to be 5MWm$^{-2}$, it is expected that >95% of the heating power will need to be exhausted via radiation.

Several potential solutions are currently being explored to address this challenge, including introducing impurities into the confined plasma to exhaust a significant fraction of the plasma heating power as

---

[†] See the author list of [Coda2017]

[*] See the author list of "H. Meyer et al 2017 Nucl. Fusion 57 102014"

radiation and alternatives to the conventional divertor configuration, such as the X-divertor [Takase2001, Kotschenreuther2007], snowflake [Ryutov2007], Super-X [Valanju2009] and X-point target [Labombard2015]. These aim to reduce the concentration of the power and particle loads to the divetor through a combination of geometry. promoting the loss of pressure and energy through atomic and molecular processes [Covele2017, Havlickova2014, Moulton2017], characteristic of the detached divertor regime and enhancing transport across the magnetic field [Ryutov2014, vijvers2014, Walkden2018, Maurizio2018, Gallo2018] to broaden the width of the SOL.

Previous studies of divertor detachment on TCV have predominantly been carried out in L-mode plasmas, including a detailed characterisation of detachment in single null configurations [Pitts2001, Pitts1999, Harrison2017, Verhaegh2018] (including the X-divertor in [Pitts2001, Theiler2017]), snowflake [labit2017, vijvers2014], and other alternative geometries [Theiler2017] including variants of the Super-X and X-point target configurations. The following contribution builds on this work to explore routes toward detachment in high (pedestal) pressure ELM-free and ELMy H-mode plasmas heated with neutral beam injection (NBI). A combination of deuterium fuelling and nitrogen seeding from the divertor is used to promote cooling of the outer divertor leg and the onset of detachment. The structure of this paper is as follows: in section 2 an overview of the experiments and key diagnostics pertinent to this study is presented. In section 3 the operational space in H-mode is characterised, including an experimental assessment of the power required to trigger an L-H transition in different divertor configurations, the pedestal properties and their relationship with the triggering of ELMs, and the limits to H-mode operation. In section 4, an overview of detachment studies in ELM-free plasmas is presented, including a comparison of using deuterium fuelling and seeding to cool the outer divertor and varying the poloidal flux expansion at the outer divertor, a characterisation of the divertor power and particle loads, impurity emission from the divertor and the global power balance of the plasma, as well as an assessment of changes in the pedestal profiles and changes in core confinement. In section 5, an overview of ELMy H-mode experiments is presented, where nitrogen seeding is used to promote detachment, with a similar structure to the analysis applied to the ELM-free experiments. In section 6, key observations from these experiments are summarised, similarities and differences identified between observations of detachment in ELM-free, ELMy H-mode and L-mode plasmas and a motivation for future experiments is given.


## 2. Overview of Experiments and Key Diagnostics

The TCV (Tokamak à Configuration Variable) tokamak [Coda2017, Fasoli2015] at EPFL is a conventional aspect ratio device (R/a = 0.88/0.25 ~ 3.5) with toroidal field ~ 1.44T and extremely high flexibility to vary the plasma shape, afforded by 16 independently controlled poloidal field coils and an open vessel structure. Recent improvements to TCV include a Neutral Beam Injector (NBI) that can inject up to 1MW of power at 25keV [Coda2017, Karpushov2017] used extensively in this study.

TCV contains an extensive array of divertor diagnostics, summarised in Figure 1 including 114 Langmuir probes (LPs) mounted in the inner and outer walls and the floor of the divertor [Pitts2003, Fevrier2018], normally swept with a frequency of 330Hz over a voltage range of -120V to +80V. The inner and outer strike points are monitored with two infra-red (IR) cameras [Maurizio2018] with a frame rate up to 25kHz. Estimates of the radiative losses and their distribution are provided by 8 gold foil pinhole cameras with 8 channels per camera [Veres2007], tomographic reconstructions of the bolometer data are routinely performed to estimate the radiation emissivity across the device. Over the course of this study, 2 filtered camera diagnostics, MSI [Linehan2018] and MANTIS [Vivjers2017] have been in use, mostly to view the lower divertor volume to monitor the spatial distribution of spectral emission lines, typically from the deuterium Balmer series, and low charge state of carbon, helium and nitrogen. The data presented here include tomographic reconstructions of uncalibrated spectral line emissivities of impurity line emission (filtered for a CIII multiplet at 464.74nm, 465.03nm, 465.14nm with a

contribution from a NII 463.31nm line) on an unstructured triangular mesh with a typical cell size of ~5mm that conforms with the poloidal cross-section of the TCV inner wall. The interpretation of the CIII filtered data from these experiments differs from previously reported findings [Harrison2017, Theiler2017, Reimerdes2017] where fuelling was applied to detach the divertor, and the movement of the edge of the CIII emitting region from the target toward the X-point was used as a means of assessing the cooling of the divertor, and by extension the proximity to detachment. In several of the experiments reported here, nitrogen seeding is used, which results in additional line emission within the bandpass of the currently used CIII filter, thereby complicating the interpretation of the data. The effect of this additional impurity contribution to the camera data was estimated by performing a comparison with measurements of the intensity of the same spectral region with a multi-chord spectrometer named DSS [Verhaegh2017] to independently measure the spectral emission within the bandpass of the filter, for comparison with purely CIII and NII emission estimated with the spectrometer. This comparison is shown in Figure 2, where it is found that there is generally good agreement between the measured emission region between the camera and spectrometer, and with the CIII emission. However it is possible that under certain conditions, such as experiments with higher nitrogen seeding rates, the NII contamination does play a more significant role. As a result, the uncertainty in the estimated impurity front location reported here is given as ±2cm (compared with a typical poloidal divertor leg length of ~35cm), larger than the spatial resolution of the measurement and the data are referred to as the impurity emission front.

Routine measurements of the upstream electron temperature and density profiles are provided by a Thomson scattering system [Hawke2017] containing 3 20Hz Nd:YAG lasers and a vertical spatial resolution that varies from 12mm to measure the steep pedestal profiles to 36mm in locations typically monitoring the confined plasma. Radial profiles of the ion temperature profiles in the core are provided by a Charge-Exchange Recombination Spectroscopy (CXRS) system.

These experiments studied variants of the single null divertor configuration in an ELM-free H-mode scenario with a plasma current, $I_p$ of 340kA ($q_{95}$ ~2.4) and 200kW of NBI heating and thre ELMy H-mode scenario with $I_p$ = 210kA ($q_{95}$ ~3.8), 170kA ($q_{95}$ ~ 4.6) and 140kA ($q_{95}$ ~ 3.9) and 1MW of NBI heating. In all cases, the ion $\nabla B$ drift is directed toward the primary X-point, as this is favourable for H-mode access; this differs from the majority of previously reported L-mode detachment experiments [Theiler2017, Harrison2017, Pitts2001, Verhaegh2017] and is expected to alter the onset and evolution of detachment via changes in transport due to cross-field drifts [Groth2011, Christen2017] and other effects. Unless otherwise stated, gas puffing into the divertor from valves situated near the floor of TCV consisted of deuterium fuelling directed toward the SOL of the outer leg and nitrogen seeding directed into the private flux region.


## 3. H-mode Operating Space

This section summarises findings from experiments to estimate the power crossing the separatrix required to trigger an L-H transition and its variation with the divertor configuration, the limits to H-mode operation and the parameter space where operation in ELMy and ELM-free H-mode regimes is possible. This information is summarised in a schematic representation of the operating space of the scenarios studied in terms of quantities most relevant to divertor physics studies, including the parallel heat flux, radiated power fraction and the upstream separatrix electron density, which effectively act to constrain the level of detachment that can be achieved whilst operating in H-mode.


### 3.1 Access to H-mode

Plasma operation in H-mode requires the power crossing the separatrix reach (or exceed) a threshold value in order to trigger the transition from L-mode. This threshold power was estimated in TCV experiments by ramping the NBI power from 0.1MW to 1MW over 700ms, slow enough that effects due to the finite energy confinement time (~few ms) and fast ion slowing down time (~10 ms [Karpushov2011]) can be neglected in the forthcoming analysis. The total plasma heating power is calculated from a sum of the ohmic heating due to the plasma current and finite plasma resistivity and the NBI power absorbed by the plasma, estimated from ASTRA [Pereverzev2002 Karpushov2015] simulations using measured plasma profiles as input. Using this approach, the power required to trigger an L-H transition was estimated in 210kA single null plasmas where the poloidal flux expansion at the outer divertor, henceforth referred to as fx, was varied from 4 to ~8.5 and the major radius of the strike point was 0.75m. Furthermore, threshold measurements were made in configurations where the strike point major radius was increased to $R_T$ ~ 1.06m and fx ~ 2.3 and in the snowflake minus configuration.

These findings are summarised in Figure 3, showing the variation in the L-H threshold power with the line average density for the divertor configurations considered. Comparison is made with previous measurements in ohmic and ECRH heated plasmas [Piras2010], which suggests the data collected in this study reside close to the density at which the threshold power is at a minimum. The data from the single null configuration with fx ~ 6.5 exhibit a weaker variation with decreasing density compared with the data obtained using ECRH heating. Furthermore, power threshold estimates in these divertor configurations over the range of line average density spanning $5\text{-}6\times10^{19}$ $m^{-3}$ suggest that divertor geometry does not significantly influence the threshold power. However, there is currently insufficient data to ascertain whether the divertor configuration affects the threshold power over a wider range of operating conditions.


## 3.2 Limits to ELMy H-mode operation

In order to achieve quasi-stationary conditions in H-mode, a regularly ELMing or ELM-free or suppressed regimes with sufficient transport from the edge into the SOL is required. In the ELM-free case studied here, the line average density continually rises through the H-mode phase at a rate of ~$7\times10^{20}$ $m^{-3}$/s until a disruptive limit is reached, which is described in more detail in the next section. Therefore, in the absence of ELM suppression techniques in TCV with sufficient transport to regulate the density, it is desirable to achieve and maintain a steady ELMing regime in attached and detached divertor conditions.

In the ELMy H-mode plasmas studied here, excessive deuterium gas fuelling can result in a transition to an ELM-free regime and a loss of quasi-stationarity or a back-transition to L-mode. To quantify the domain of ELMy and ELM-free regimes, in terms of the pedestal top temperature and density $T_e^{ped}$ and $n_e^{ped}$ respectively, a database was compiled of Thomson scattering measurements of pedestal temperature and density profiles in both ELMy and ELM-free regimes. Estimates of the pedestal height and width were obtained by fitting mtanh functions [Dickinson2011] to these profiles. The resulting database in shown in Figure 4, showing a clear delineation between the ELMy regime where $n_e^{ped} \leq 5\times10^{19}$ $m^{-3}$ and a transition to an ELM-free regime at higher densities, no such threshold is apparent in terms of $T_e^{ped}$. This threshold is further illustrated in Figure 4, where a high current ELMing plasma ($I_p = 390$kA, $q_{95} = 2.10$) is fuelled to raise the pedestal density, which causes a transition to ELM-free when the pedestal top density is above $5\times10^{19}$ $m^{-3}$. It is not clear whether the pedestal top density or another correlated quantity, such as the separatrix density, is responsible for setting this limit. This threshold imposes a constraint on the highest achievable density at the separatrix for a given density gradient. If it is assumed that the separatrix density is at most 50% of $n_e^{ped}$, this suggests it cannot exceed ~$2.5\times10^{19}$ $m^{-3}$ unless this constraint is relaxed, e.g. by modifying the plasma shaping to promote the triggering of ELMs or increasing the heating power.

### 3.3 H-mode Operating Limits

The ELM-free plasmas studied here are characterised by a steady rise of the line average density until the plasma disrupted, typically due to a loss of control of the vertical position of the plasma. In the absence of fuelling and seeding from the divertor, these disruptions would typically occur at ~80% of the Greenwald density limit [Greenwald2002], defined as $\overline{n_e}(10^{20}m^{-3}) = \frac{I_p(MA)}{\pi a^2(m^2)}$ where Ip is the plasma current and a is the minor radius of the core plasma. The addition of deuterium fuelling and nitrogen seeding alone reduced this limit to ~76% and ~70% respectively, and a combination of fuelling and seeding resulted in the limit lowering slightly to ~69%.

In the ELMy H-mode regime, the principal limits are set by the power required to stay in H-mode and the transition to ELM-free or L-mode. Strong nitrogen seeding leads to a steady reduction of the ELM amplitude and eventually a transition back to L-mode. This behaviour is observed in these experiments when the proportion of the power crossing the separatrix, $P_{SOL}$ radiated in the SOL and divertor (i.e. $P_{rad}^{div\text{-}SOL}/P_{SOL} = f_{rad,SOL}$) is ~20-30% (as shown in Figure 5 and Figure 20). The highest achievable density at the sepratrix is set by the transition to an ELM-free regime when $n_e^{ped} > 5\text{x}10^{19}$ m$^{-3}$.

### 3.4 Overview of the H-mode operating space

Taking the considerations mentioned in the preceding sections into account, the H-mode operating scenarios for these experiments, in terms of quantities relevant for studies of divertor detachment, is shown in Figure 5. The upstream density is estimated from performing mtanh fits to the pedestal temperature and density profiles, and enforcing the constraint that the separatrix temperature agree with estimates from the two-point model [Harrison1990], which requires the upstream parallel heat flux ($q_{||}$), upstream separatrix density and the radial width of the SOL $\lambda_q$, as inputs. The parallel heat flux is estimated from the expression [Reimerdes2017a]:

$$q_{||} = \frac{B_{tot,u}}{B_{p,u}} \frac{c_{div} P_{SOL}}{2\pi R_u \lambda_q}$$

Where $B_{tot,u}$ and $B_{p,u}$ are the total and poloidal magnetic field components at the outer mid-plane at major radius $R_u$, $c_{div}$ is the proportion of the power crossing the separatrix, flowing to the divertor leg studied, $P_{SOL}$ is the power crossing the separatrix and $\lambda_q$ is the width of the SOL at the outer mid-plane. $P_{SOL}$ is calculated from considerations of the global power balance, discussed in the following sections. In ELMy scenarios, the inter-ELM power balance is estimated using foil bolometer measurements of the radiation between ELMs and the average energy loss due to ELMs estimated by the change in diamagnetic flux. Estimates of the separatrix temperature, and subsequently the density, are iterated until convergence. This allows operating conditions in the absence and presence of additional gas fuelling and seeding to promote detachment to be compared between the H-mode scenarios explored and with the detachment threshold observed in 340kA ohmic L-mode plasmas studied previously [Harrison2017, Verhaegh2017]. It is found that the application of additional fuelling and seeding does not significantly influence the parallel heat flux, but can increase both $f_{rad}$ and the upstream density by a factor ~2 (see Figure 6).

## 4. ELM-free H-mode Experiments

### 4.1 General observations

As outlined in Figure 5 and Figure 6 in previous sections, ELM-free H-mode scenarios are characterised by relatively high pedestal top density, $n_e^{ped} > 5 \times 10^{19}$ m$^{-3}$, moderate temperature $100 \text{eV} < T_e^{ped} < 180 \text{eV}$ and parallel heat flux ~19MWm$^{-2}$, meaning they are amenable to approaching the conditions required for divertor detachment. An overview of a typical ELM-free H-mode plasma with fuelling from the lower divertor is shown in Figure 6, showing a strong increase in the line average density from ~$1.0 \times 10^{20}$ m$^{-3}$ up to $1.7 \times 10^{20}$ m$^{-3}$ and a corresponding increase in both the ohmic heating power, due to the higher electrical resistivity of the core plasma at fixed plasma current, and total radiated power. The plasma stored energy and energy confinement time, $\tau_E$, (calculated from the ratio of the plasma stored energy and the total heating power) is approximately constant throughout the H-mode phase, resulting in the H factor (the energy confinement time normalised to the predicted value based on the IPB98y,2 scaling [Kardaun1999]) reducing from ~0.8 to 0.6, as the scaling law assumes that $\tau_E$ scales with density as $n_e^{0.41}$, which is not evident in these experiments. The total particle flux to the inner and outer divertors is approximately constant throughout the H-mode phase unless strong fuelling and seeding are applied.

## 4.2 Effects of Fuelling and Seeding

### 4.2.1 Global power balance

In order to quantify the progress toward reaching divertor detachment, it is instructive to start from the consideration of the main sources and sinks of power to and from the plasma respectively. The main sources of power to the plasma are from ohmic (resistive) heating $P_{ohm}$ and neutral beam injection $P_{NBI}^{inj}$. Estimates of the ohmic heating power are derived from LIUQE [Moret2015] equilibrium reconstructions, and the proportion of the injected NBI power absorbed by the plasma is estimated from a database of ASTRA simulations compiled to derive the L-H threshold power to estimate a scaling of the fraction of the neutral beam power delivered by the ion source absorbed by the plasma $P_{NBI}^{inj}$, subtracting losses due to charge-exchange and orbit losses, $f_{abs}$. It was found to vary most strongly with line average density, $\overline{n_e}$, according to the relationship $f_{abs} = 0.73 - e^{-0.5 \times 10^{19} \overline{n_e}}$, which is to be expected given that the peaking of the temperature and density profiles is similar in the shots in this study. The primary power sinks are due to radiation, both inside and outside the core ($P_{rad}^{core}$ and $P_{rad}^{div-SOL}$), and the rate of change of stored energy $\frac{dW}{dt}$, which plays a significant role immediately following the L-H transition. To quantify the progress toward detachment, the power crossing the separatrix is estimated according to $P_{SOL} = P_{ohm} + f_{abs} P_{NBI}^{inj} - \frac{dW}{dt} - P_{rad}^{core}$, which is the power that must be exhausted in the divertor and SOL or convected by the plasma to plasma-facing surfaces, and the exhaust power $P_{SOL} - P_{rad}^{div-SOL}$, which estimates only the power deposited from the plasma to the surfaces.

An overview of the power balance of a typical fuelled and nitrogen seeded ELM-free shot is shown in Figure 7 to illustrate the time evolution of the power sources and sinks. In the 1-2ms following the L-H transition, the plasma stored energy increases rapidly, resulting the dW/dt term having a strong impact on the overall power balance. Following this phase, the sources of power rise throughout the ELM-free phase due to an increase in the ohmic heating power. This rise is compensated by an increase in the radiation both inside and outside the core that cause the exhaust power to roll over toward the end of the H-mode phase.

The evolution of the radiation losses and their distribution has been studied in detail by analysing the tomographically inverted foil bolometer data. The majority of the increase in radiation originates from the confined plasma, irrespective of the level of fuelling or seeding applied, and is likely related to the density continually increasing throughout the H-mode phase and the ingress of impurities due to sputtering from the carbon plasma-facing tiles. Moreover, as the divertor cools due to the injection of

nitrogen, the radiation from the outer leg recedes from the strike point toward the X-point and a commensurate increase in the radiation emissivity along the outer leg in the vicinity of the X-point, as shown in Figure 8. A quantification of the power radiated from the different regions of the plasma is shown in Figure 9 for the nitrogen seeded shot discussed in Figure 7 and Figure 8, confirming that the radiation from the core increases most quickly, from ~30% of the total radiated power at the start of the H-mode phase to ~50% just prior to a disruption. The total power radiated in the inner and outer divertors is approximately constant throughout the density ramp, while the radiation at the X-point increases by 50% (although its contribution to the total radiated power is less than 8% throughout the H-mode phase). The inverted bolometer data suggest that this is due to radiation emissivity increasing, mitigating the decrease in the radiating volume as the front moves toward the X-point.

Inverted impurity emission and deuterium Balmer γ emission profiles from the MSI imaging diagnostic at the start and end of the fuelling and seeding phase of a shot with the highest nitrogen seeding rate is shown in Figure 10. At the start of the fuelling and seeding phase, the impurity emission extends along the outer leg from the X-point to the vicinity of the strike point, then recedes toward the X-point prior to a disruption. The movement of the impurity emission toward the X-point is indicative of the radiation front receding in a similar manner, as previous L-mode experiments [Theiler2017] found the two to be in reasonable agreement. The distribution of the deuterium Balmer γ emission is broadly unchanged but has a lower brightness at the end of the seeding phase. This reduction in the Balmer line emission is instructive because if the population of the deuterium atomic states is dominated by electron impact excitation (as opposed to volume recombination), the line brightness is proportional to the ionization source, which in turn governs the total particle flux to the divertor.

However, the total radiation outside the confined plasma steadily increases with time due to emission from the SOL in the vicinity of the outer mid-plane and the far scrape-off layer, which could be due to sputtering of impurities from plasma-surface interactions or artefacts in the tomographic reconstructions.


### 4.2.2 Pedestal profile evolution

The evolution of these ELM-free H-mode shots is rapid, typically lasting for less than 200ms and is characterised by a rapid increase in the line average density. During the H-mode phase, the electron temperature and density profiles also changes substantially. A typical example of the evolution of the pedestal profiles is shown in Figure 11, where mtanh fits to the Thomson scattering data during the fuelling and seeding phase are presented, using the two point model to constrain the electron temperature as described in section 3.4. The pedestal top electron density is found to increase by ~30% and the separatrix density to increase by a factor of ~2, and are found to be independent of the level of fuelling or seeding. Conversely, the electron temperature at the pedestal top decreases by ~15% and the separatrix temperature is approximately constant, as the variations in $P_{SOL}$ are sufficiently small that they do not significantly modify the separatrix temperature. The gradient in the edge electron temperature profile is also observed to decrease over time, concomitant with a 20% reduction in the temperature close to the magnetic axis, from ~500eV at the start of the H-mode phase, accompanied by a commensurate increase in density.


### 4.2.3 Outer Divertor Power and Particle Loads

The influence of deuterium fuelling on the power and particle loads to the outer divertor were studied by running similar discharges with different levels of fuelling into the SOL region on the floor. The results of this scan are shown in Figure 12, which shows the total power loads to the outer divertor, estimated using IR thermography and Langmuir probe arrays, and total particle loads estimated by the

probes. The power deposited to the divertor $q_{dep}$ is estimated from the Langmuir probe data using the relationship $q_{dep} = e n_e^t c_s^t \left( \gamma T_e^t + E_{pot} \right)$ where $c_s$ is the ion acoustic velocity, given by $\sqrt{\left( T_e^t + T_i^t \right)/m_i}$ where the ion and electron temperatures are assumed equal, $E_{pot}$ is the potential energy of each ion, the sum of the hydrogen ionisation energy (13.6eV) and half of the Franck-Condon molecular dissociation energy (2.2eV), $\gamma$ is the sheath heat transmission factor, which is typically taken to be 5 at TCV, based on comparison between divertor power load measurements from Langmuir probes and IR thermography [Marki2007].

Immediately following the L-H transition, both the power and particle fluxes fall transiently, due to an increase in stored energy. Following this phase, it is found that increasing fuelling can reduce the power loads by ~30%, although there does not appear to be a significant reduction in either total or peak ion flux.

The effect of a combination of fuelling and seeding was studied in similar plasmas as those in the fuelling scan, as illustrated in Figure 13. In these shots, fuelling into the SOL at a rate of $9x10^{20}$ $D_2$/s was used in conjunction and nitrogen injected into the private flux region. The timing of the L-H transition was not perfectly reproducible, so the timing of the fuelling and seeding waveforms differ between shots. The total divertor power load is reduced by ~50% in the case with the highest level of seeding, compared with the shot with no seeding. There is also evidence of a modest reduction in the total ion flux, which is mostly due to a reduction in the peak of the profile. This would indicate that the divertor is in a state of partial detachment in terms of the power flux reaching the divertor, but less so in terms of the particle flux. This would indicate that nitrogen seeding is more effective than fuelling in mitigating the divertor particle and heat flux. A comparison of these results with scalings of the proximity to detachment with machine operating parameters (e.g. [Kallenbach2015, Kallenbach2016]) is not currently possible, as the pressure gauge measurements do not have a sufficiently short time response to characterise the ELM-free phase.

### 4.2.4 Impurity Line Emission

In previous L-mode detachment studies on TCV, the movement of the impurity emission front from the target to the X-point on the approach to detachment has been used to infer the cooling of the divertor leg and the proximity to the onset of detachment. For example, in Figure 14 the emission front moves mid-way from the target to the X-point when the total ion flux to the outer divertor starts to roll over. This approach has been applied to estimate the efficacy of fuelling and seeding to cool the outer divertor leg in the shots presented in this section. The time evolution of the position of the impurity emission front is shown in Figure 15, plotted as a function of time since the L-H transition. It is observed that the application of fuelling alone is sufficient for the emission front to move from the target to half way up the leg, close to the position where a roll-over in the divertor ion flux occurs in L-mode experiments. The application of increasing levels of seeding results in the emission front moving closer to the X-point, and more quickly, with increasing nitrogen seeding. On this basis, it appears that nitrogen seeding is more efficient at cooling the divertor than fuelling. However, if the front location in these shots is compared with respect to the number of electrons injected during the H-mode phase, it is found that both fuelling and seeding have a similar effect.

### 4.5 Influence of Outer Divertor Poloidal Flux Expansion

In previous L-mode experiments using fuelling to reach divertor detachment [Theiler2017, Reimerdes2017], the poloidal flux expansion at the outer divertor was found to influence the highest achievable reduction in the divertor ion flux whilst the detachment threshold, in terms of core line

average density was unchanged. In the present H-mode experiments, fuelling and seeding are applied to shots with fx = 3.5, 6.5, 10, representative equilibria are shown in Figure 16. In both the fuelled and nitrogen seeded shots, the time evolution of the outer divertor heat and particle flux profiles did not vary significantly as a result of varying fx. However, there was a net reduction in the measured power and particle loads with increasing fx, which is thought to be due to changes in the power and particle flux distribution between the inner and outer divertors observed in [Maurizio2018]. Furthermore, comparison of the impurity emission front movement with fuelling and seeding (data from the fuelling scan are shown in Figure 17) did not indicate that fx strongly influences the cooling of the divertor leg.

## 5. ELMy H-mode Experiments

### 5.1 General observations

Unlike the ELM-free experiments discussed previously, ELMy H-modes are normally quasi-stationary, with ELMs providing sufficient particle transport to regulate the particle content of the core. In these experiments, nitrogen seeding was used to promote cooling of the outer leg, and thereby approach detachment, in 3 scenarios of different plasma current, 210kA, 170kA and 140kA, with equilibria shown in Figure 18. From the consideration of the pedestal temperature and density discussed in section 3.2, the higher pedestal temperature and lower density would indicate these scenarios are more challenging to detach than the ELM-free shots.

The time evolution of a 210kA discharge with strong nitrogen seeding into the private flux region is shown in Figure 19. The plasma enters a phase with regularly spaced ELMs at 0.95s, shortly before the introduction of nitrogen seeding at 1.01s. The seeding results in a factor ~2 increase in the total radiation, a steady reduction of the ELM amplitude and a ~30% reduction in the energy confinement time relative to the IPB98(y,2) scaling (although the stored energy is constant), and eventually a back transition to L-mode.

### 5.2 Global power balance

The terms in the global power balance in these ELMy H-mode plasmas are similar to those considered in the ELM-free cases discussed in the previous section except that the average power transported through the SOL by ELMs should also be accounted for. The ELM losses are estimated using the difference between measurements of the stored energy from a diamagnetic loop before and after an ELM and after any over-shoot of the measurement. A time average of the ELM energy loss is estimated by performing a linear fit to the product of the energy loss per ELM and the ELM frequency over the ELMing phase. The radiation losses between ELMs are estimated by applying a minimum moving window filter to the analysed bolometer data, with a window at least twice as wide as the ELM duration.

The global power balance of an ELMy H-mode shot with strong nitrogen seeding is shown in Figure 20. The application of seeding leads to an increase in radiation both inside and outside the confined plasma in equal measure, however $P_{SOL}$ is maintained at ~700kW as the increase in core radiation is compensated by an increase in the ohmic heating power. The estimated power deposited on plasma-facing surfaces, referred to as the inter-ELM exhaust power in Figure 20, is reduced from ~600kW to ~500-550kW due to the increased radiation in the divertor and SOL as a consequence of the nitrogen injection. During the nitrogen seeding phase, the ELM amplitude diminishes until the H-mode period ends with a back-transition to L-mode.

### 5.3 Pedestal profile evolution

In the shot discussed in the previous section, strong nitrogen seeding resulted in the loss of H-mode. An examination of the pedestal electron density and temperature profiles during this phase, in a lower $I_p$ shot (140kA compared with 210kA in the shot discussed in the previous section) where the pedestal position is optimal for Thomson scattering measurements is shown in Figure 22, indicating no clear trend in the electron density profiles but a gradual reduction in the pedestal top temperature from ~340eV at the start of the seeding phase to ~220eV before the back-transition to L-mode. The separatrix electron temperature and density do not exhibit any clear trends, with the separatrix electron density varying from ~1.5-2.5x10$^{19}$ m$^{-3}$ measured at random phases during the ELM cycle. The separatrix electron temperature is constrained to conform with estimates from the two-point model, which vary from 60-70eV between scenarios. As $P_{SOL}$ is approximately maintained during the seeding phase, the two-point model, including the measured radiation losses, would not predict changes in the upstream temperature.

## 5.4 Outer Divertor Power and Particle Loads

The main effect of nitrogen injection into the ELMy H-mode plasmas considered here is to strongly reduce electron temperature profile across the outer divertor. This is illustrated in Figure 23, which shows the time evolution of the total ion flux to the outer divertor and profiles of the ion saturation current density, electron temperature before and after the application of nitrogen seeding.

Comparison of the target profiles before and after the application of seeding shows that the most pronounced effect is on the electron temperature profile. The initially peaked profile, with a maximum temperature of ~20eV flattens, and the peak temperature drops to ~5eV. Conversely, the electron density profiles are similar, if slightly elevated, after the seeding is applied. This is unlikely to be due to the additional electrons introduced by the nitrogen seeding (which is ~1% of the particle flux to the divertor), and could be due to reduction in the target pressure being less than the reduction in temperature. The peak plasma pressure at the outer target is reduced by a factor ~5, whereas the upstream temperature is broadly unchanged, indicating the plasma in the vicinity of the separatrix is partially detached [Loarte1998]. The reduction in the electron temperature profile leads to a factor ~2 reduction in the total power deposited to the outer divertor.

## 5.5 Influence of Outer Divertor Target Major Radius

In previous L-mode experiments using fuelling to detach the outer divertor [Theiler2017] it was found that varying the major radius of the outer strike point did not significantly affect the detachment characteristics. This is contrary to predictions from a modified two-point model [Petrie2013] that predict the electron temperature and density at the target vary with the ratio of the upstream and target major radii $R_u$, $R_t$ respectively, according to $T_e \propto \left(\frac{R_u^2}{R_t^2}\right)$ and $n_e \propto \left(\frac{R_t^2}{R_u^2}\right)$. To ascertain whether this behaviour is evident in ELMy H-mode experiments, shots were carried out with the strike point major radius $R_T$ placed at 0.75m and 1.03m and $I_p$ = 170kA ($q_{95}$ = 4.1), 1MW of NBI heating and similar Greenwald fraction ($n_G$ ($R_T$ = 0.75m) ~ 0.37, $n_G$ ($R_T$ = 1.03m) ~ 0.42) and poloidal flux expansion at the outer divertor ($f_{exp}$ ($R_T$ = 0.75m) ~ 2.4, $f_{exp}$ ($R_T$ = 1.03m) = 2.2), as shown in Figure 24. Nitrogen seeding into the private flux region was used to cool the divertor to promote detachment of the outer divertor.

Our primary measure of the progress toward detachment is the location of the impurity emission front, as was the case in the previous L-mode studies. Measurements of the outer divertor particle loads were not available because the Langmuir probe array does not currently extend to cover the strike point beyond a major radius of 0.965m, however the probe coverage will be extended in the future

[Reimerdes2017a]. The time evolution of the impurity emission front location in these cases is shown in Figure 25. The impurity emission front moves from the target toward the X-point following the start of the nitrogen injection. These data have been filtered to show measurements between and during ELMs, as ELMs move the emission front to the divertor surface irrespective of the location of the front between ELMs, consistent with the ELMs 'burning through' the cooling divertor leg. In between ELMs, the difference in the impurity front movement between the smaller and larger $R_T$ cases is rather subtle, which was also observed in L-mode experiments. The duration of the ELMy H-mode phase in the presence of nitrogen seeding is also similar in both cases, lasting ~70ms.

The impurity emission front starts to move away from the target at the same time in both cases, although the speed of the front movement appears to be slower in the larger $R_T$ case, taking 25ms to move from the target to ~10cm from the X-point in the larger $R_T$ experiment, compared with 19.5ms at lower $R_T$. It is possible that the slower motion of the front location in the larger $R_T$ case is due in part to the higher ELM frequency (~100Hz compared with ~92Hz in the lower $R_T$ case), however the data suggest that the front location after an ELM can return to its pre-ELM position in the time between frames, 2.5ms, so this effect alone is unlikely to explain this behaviour.


## 6. Summary & Conclusions

Access to partial detachment in ELM-free and ELMy H-mode TCV discharges, where there is a noticeable reduction in the outer divertor power load, has been explored using fuelling and nitrogen injection from the divertor in a range of divertor configurations. A characterisation of the H-mode operating space has been carried out, in terms of assessing the conditions required to enter and sustain H-mode. It has been observed that the heating power required to cross the L-H transition threshold, where the density is close to the minimum in the $P_{L-H}/n_e$ curve, is relatively insensitive to the outer target poloidal flux expansion or major radius in the single null configuration, nor is there a large difference in threshold power between these variants on the single null and the snowflake minus configurations studied.

The limits to quasi-stationary H-mode operation have been quantified, including transitions from ELMy to ELM-free conditions and the disruptive limits in ELM-free plasmas and back transition to L-mode in ELMy scenarios. ELM-free H-mode scenarios have some positive properties to aid progress toward divertor detachment, including moderate separatrix electron temperature (~40-50eV) and relatively high separatrix density (> $2.5\times10^{19}$ m$^{-3}$), however, the ELM-free phase typically have a duration of <200ms, which decreases when fuelling or seeding is applied. Using a combination of fuelling and nitrogen seeding, a small reduction in the peak and total ion flux to the outer divertor was observed, and the total power deposited to the outer divertor was reduced by a factor ~2. A comparison of fuelling and seeding on divertor cooling, quantified in terms of movement of the impurity radiation front from the target toward the X-point was carried out, showing that seeding resulted in stronger cooling of the divertor, but the two gases have the same effect on the impurity front location in terms of the number of electrons injected (see Figure 15). The effect of poloidal flux expansion on divertor cooling was studied in both fuelled and nitrogen seeded experiments, which was not found to play a strong role.

Nitrogen seeding in ELMy H-mode plasmas was found to significantly reduce the electron temperature at the outer divertor, reducing the peak temperature by a factor of ~3-4, while the electron density profile was broadly similar, and slightly elevated near the peak of the profile, indicating that the outer divertor is in a state of partial detachment. A factor ~2 reduction in the total power load to the outer divertor between ELMs was observed. The effect of the outer target major radius on the movement of the impurity radiation was explored in experiments with the strike point at R= 0.75m and 1.03m. The movement of the impurity radiation front from the target toward the X-point was found to be ~20% slower when the strike point was moved to larger radius, which could suggest that the front is less

sensitive to changes in the divertor conditions. Nitrogen seeding results in a steady reduction in the ELM amplitude and a back-transition to L-mode. The duration of the ELMy H-mode phase was found to be independent of the major radius of the strike point.

Analysis of both the ELMy and ELM-free shots indicate that strong fuelling and seeding result in the loss of H-mode and shorter H-mode phases respectively, which suggests that the main impediment to making further progress towards achieving greater divertor heat and particle flux mitigation is set by the requirement to remain in H-mode and preferably in an ELMy, quasi-stationary state. Further progress looks likely when the new baffle structures are installed in TCV [Fasoli2015, Reimerdes2017a] that will promote radiative losses by increasing divertor neutral compression and elevating the divertor electron density (as the radiated power from a given species is proportional to $n_e^2$ at fixed concentration this could be an important effect) and increased neutral beam heating may elevate the pedestal top density before a transition from ELMy to ELM-free H-mode occurs.

This work provides a basis for future detachment studies in H-mode on TCV, including extending this work to include other alternative divertor concepts such as the double null, snowflake and X-point target at higher heating power and to continue explore the role of the divertor configuration in mediating ELM heat and particle fluxes. The excellent diagnostics capabilities can be further leveraged to characterise the plasma conditions in attached and detached conditions to allow for detailed modelling studies to facilitate greater understanding.

**6. References**

[Piras2010] F. Piras, S. Coda, B. P. Duval, B. Labit, J. Marki, S. Yu. Medvedev, J.-M. Moret, A. Pitzschke, O. Sauter, Phys. Rev. Lett. **105**, 155003 (2010)

[Martin2008] Y. R. Martin, T. Takizuka et al., J. Phys.: Conf. Ser. **123** 012033 (2008)

[Harrison2017] J.R.Harrison, W.A.J.Vijvers, C.Theiler, B.P.Duval, S.Elmore, B. Labit, B.Lipschultz, S.H.M.van Limpt, S.W.Lisgo, C.K.Tsui, H.Reimerdes, U.Sheikh, K.H.A.Verhaegh, M.Wischmeier, Nuclear Materials and Energy 12 (2017) 1071–1076

[Pitts1999] R. A. Pitts, A. Refke, B. P. Duval, I. Furno, B. Joye, J. B. Lister, Y. Martin, J.-M. Moret, R. Romers, H. Weisen, J. Nucl. Mater. **266-269** (1999) 649-653 – Neon detachment

[Theiler 2017] C. Theiler, B. Lipschultz, J. Harrison, B. Labit, H. Reimerdes, C. Tsui, W. A. J. Vijvers, J. A. Boedo, B. P. Duval, Nucl. Fusion **57** 072008 (2017) – L-mode alternative divertor configurations

[Pitts2001] R. A. Pitts, B. P. Duval, A. Loarte, J.-M. Moret, J. A. Boedo, D. Coster, I. Furno, J. Horacek, A. S. Kukushkin, D. Reiter, J. Rommers, J. Nucl. Mater. **290-293** (2001) 940-946 – TCV L-mode paper

[Reimerdes2017] H. Reimerdes et al., Nucl. Fusion **57** 126007 (2017)

[Reimerdes2017a] H. Reimerdes et al., Nucl. Mat. Energy **12** (2017) 1106-1111 – TCV divertor upgrade

[Zohm2013] H. Zohm, et al., Nucl. Fusion **53** 073019 (2013) – physics guidelines for DEMO

[Labit2017] B.Labit, G.P.Canal, N.Christen, B.P.Duval, B.Lipschultz, T.Lunt, F.Nespoli, H.Reimerdes, U.Sheikh, C.Theiler, C.K.Tsui, K.Verhaegh, W.A.J.Vijvers, Nucl. Mat. Energy **12** (2017) 1015-1019

[Vijvers2014] W.A.J. Vijvers, G.P. Canal, B. Labit, H. Reimerdes, B. Tal, S. Coda, G.C. De Temmerman, B.P. Duval, T.W. Morgan, J.J. Zielinski, Nucl. Fusion **54** 023009 (2014)

[Coda2017] S. Coda et al., Nucl. Fusion **57** 102011 (2017)

[Karpushov2011] A. Karpushov et al., Fusion Eng. Des **86** 868-871 (2011)

[Karpushov2017] A. Karpushov et al., Fusion Eng. Des. **123** 468-472 (2017)

[Pitts2003] R. A. Pitts, S. Alberti, P. Blanchard, J. Horacek, H. Reimerdes, P. C. Stangeby Nucl. Fusion **43** 1145–66 (2003)

[Reimerdes2013] H Reimerdes, G P Canal, B P Duval, B Labit, T Lunt, W A J Vijvers, S Coda, G De Temmerman, T W Morgan, F Nespoli, B Tal, Plasma Phys. Control. Fusion **55** 124027 (2013) – power distribution in snowflake

[Maurizio2018] R. Maurizio, S. Elmore, N. Fedorczak, A. Gallo, H. Reimerdes, B. Labit, C. Theiler, C.K. Tsui, W.A.J. Vijvers, Nucl. Fusion **58** 016052 (2018)

[Verhaegh2017] K.Verhaegh, B.Lipschultz, B.P.Duval, J.R.Harrison, H.Reimerdes, C.Theiler, B.Labit, R.Maurizio, C.Marini, F.Nespoli, U.Sheikh, C.K.Tsuid, N.Vianello, W.A.J.Vijvers, Nucl. Mat. Energy **12** 1112-1117 (2017)

[Groth2011] M. Groth et al.,.J. Nucl. Mater. **415** S530–S534 (2011)

[Pereverzev2002] G.V. Pereverzev, P.N. Yushmanov, ASTRA, Automated System for Transport Analysis in a Tokamak, Max-Planck-Institut für Plasmaphysik, Garching, 2002,IPP Report 5/98

[Greenwald2002] M. Greenwald, Plasma Phys. Control. Fusion **44** R27 (2002)

[Wenninger2014] R.P. Wenninger et al., Nucl. Fusion **54** 114003 (2014)

[Valanju2009] P. M. Valanju, M. Kotschenreuther, S. M. Mahajan, J Canik Phys. Plasmas **16** 056110 (2009)

[Ryutov2007] D. D. Ryutov Phys. Plasmas **14** 064502 (2007)

[Dickinson2011] D. Dickinson, S. Saarelma, R. Scannell, A. Kirk, C. M. Roach, H. R. Wilson, Plasma Phys. Control. Fusion **53** 115010 (2011)

[Harrison1990] M. F. A. Harrison, E. S. Hotston, J. Nucl. Med. **176-177** 256 (1990)

[Kardaun1999] O. Kardaun, Plasma Phys. Control. Fusion **41** 429 (1999)

[Kallenbach2016] A. Kallenbach, M. Bernert, R. Dux, F. Reimold, M. Wischmeier, Plasma Phys. Control. Fusion **58** 045013 (2016)

[Karpushov2015] A.N.Karpushov, et al., Fusion Eng. Des. **96–97** 493–497 (2015)

[Moret2015] J.-M.Moret, B.P.Duval, H.B.Le, S.Coda, F.Felici, H.Reimerdes, Fusion Eng. Des. **91** 1-15 (2015)

[Takase2001] H. Takase,  J. Phys. Soc. Japan **70** 609 (2001)

[Kotschenreuther2007] M. Kotschenreuther, P. M. Valanju, S. M. Mahajan, J. C. Wiley,  Phys. Plasmas **14** 072502 (2007)

[Labombard2015] B. LaBombard et al., Nucl. Fusion **55** 053020 (2015)

[Shimada2007] M. Shimada et al., Nucl. Fusion **47** S1–17 (2007)

[Pitts2017] R. A. Pitts et al., Nucl. Mat. Energy **12** 60-74 (2017)

[Fasoli2015] A. Fasoli and TCV Team, Nucl. Fusion **55** 043006 (2015)

[Veres2007] G.Veres, R.A.Pitts, M.Wischmeier, B.Gulejova, J.Horacek, S.Kálvin, J. Nucl. Mater. **363-365** 1104-1109 (2007)

[Linehan2018] B. Linehan et al., accepted Rev. Sci. Instrum.

[Hawke2017] J. Hawke, Y. Andrebe, R. Bertizzolo, P. Blanchard, R. Chavan, J. Decker, B. P. Duval, P. Lavanchy, X. Llobet, B. Marlétaz, P. Marmillod, G. Pochon and M. Toussaint, JINST **12** C12005

[Petrie2013] T. W. Petrie Nucl. Fusion **53** 113024 (2013)

[Vijvers2017] W.A.J. Vijvers, R.T. Mumgaard, Y. Andrebe, I.G.J. Classen, B.P. Duval, B. Lipschultz JINST **12** C12058 (2017)

[Loarte1998] A. Loarte et al., Nucl. Fusion **38** 331 (1998)

[Marki2007] Marki J et al., J. Nucl. Mater. **363** 382 (2007)

[Kallenbach2015] A. Kallenbach et al., Nucl. Fusion **55** 053026 (2015)

[Fevrier2018] O. Février, C. Theiler, H. De Oliveira, B. Labit, N. Fedorczak, A. Baillod, Rev. Sci. Instrum. **89** 053502 (2018)

[Moulton2017] D. Moulton et al., Plasma Phys. Control. Fusion **59** 065011 (2017)

[Covele2017] B. Covele et al., Nucl. Fusion **57** 086017 (2017)

[Havlickova2014] E. Havlíčková et al., Plasma Phys. Control. Fusion **56** 075008 (2014)

[Ryutov2014] D. D. Ryutov, R. H. Cohen, W. A. Farmer, T. D. Rognlien, M. V. Umansky, Phys. Scr. **89** 088002 (2014)

[Walkden2018] N. R. Walkden, B. Labit, H. Reimerdes, J. Harrison, T. Farley, P. Innocente, F. Militello, "Fluctuation characteristics of the TCV snowflake divertor measured with high speed visible imaging" accepted by Plasma Phys. Control Fusion

[Gallo2018] A. Gallo et al., Plasma Phys. Control. Fusion **60** 014007 (2018)

[Christen2017] N. Christen et al., Plasma Phys. Control. Fusion **59** 105004 (2017)

**Figures**
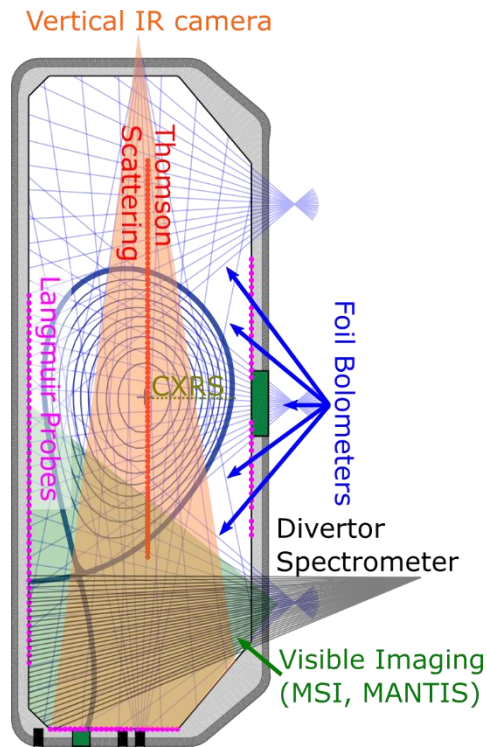


Figure 1: Overview of the main core and divertor diagnostics used in this study.
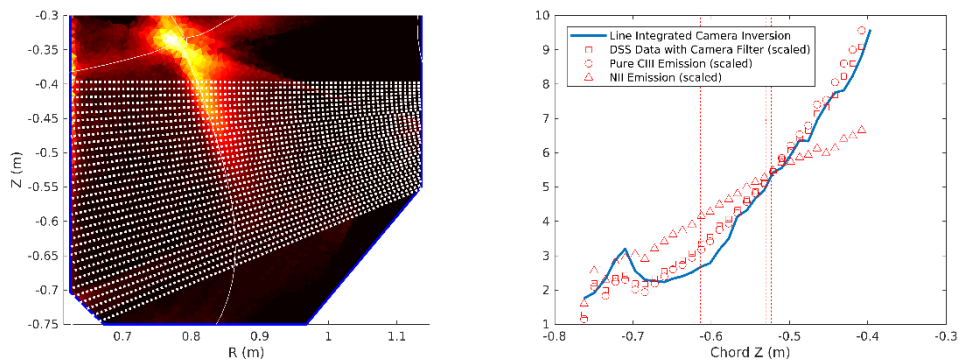


Figure 2: (Left) Inverted camera data filtered primarily for CIII emission with the DSS spectrometer viewing chords overlaid. (Right) Profiles of the emissivity shown on the left integrated along the DSS chords, the DSS emission within the CIII filter bandpass, and purely CIII and NII emission. The various front locations derived from these emission profiles, taken to be when the emission drops to 50% of the peak value, are shown as vertical lines.
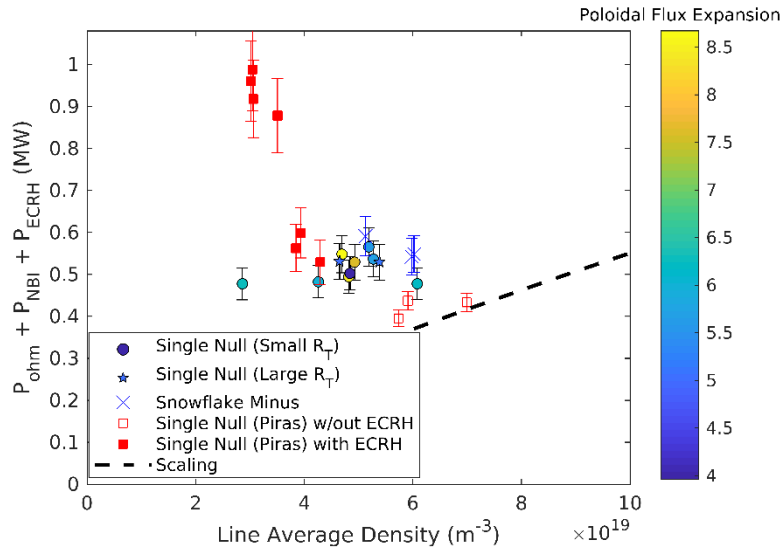
*Figure 3: Heating power applied at the L-H transition as a function of core line average density single null divertor configurations of different outer target poloidal flux expansion and major radius and snowflake configurations with NBI heating. Comparison is made with previously published data from single null ECRH and ohmic heated discharges [Piras2010] and the widely used scaling by Martin [Martin2008].*
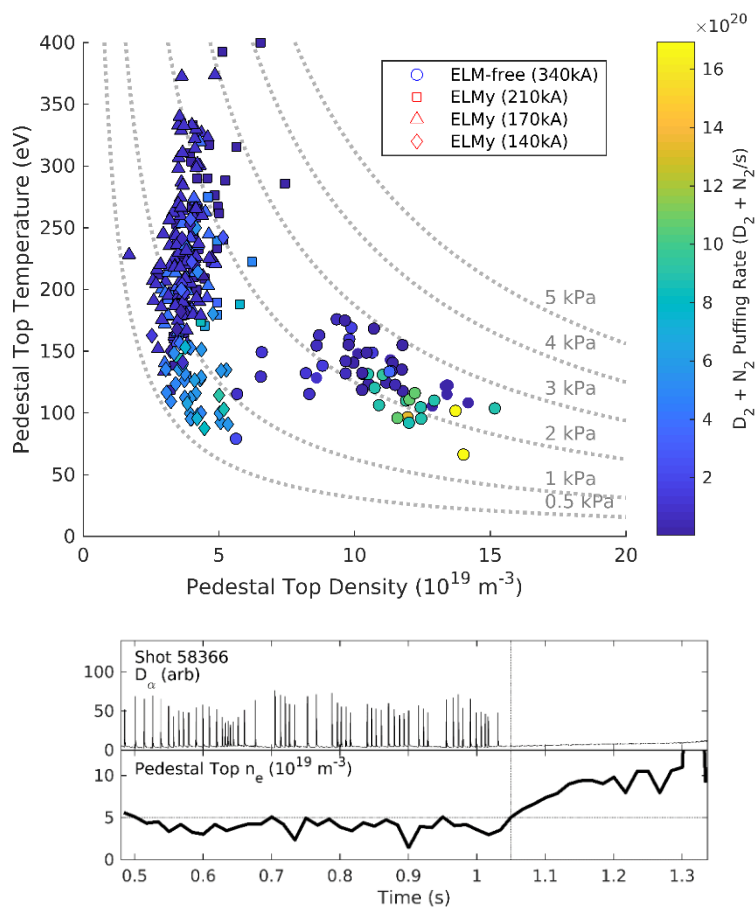


*Figure 4: Upper - Electron density and temperature at the pedestal top in ELM-free and ELMy H-mode scenarios. Lower – Transition from ELMy to ELM-free regime in a shot when the pedestal top density exceeds 5x10^19 m^-3.*
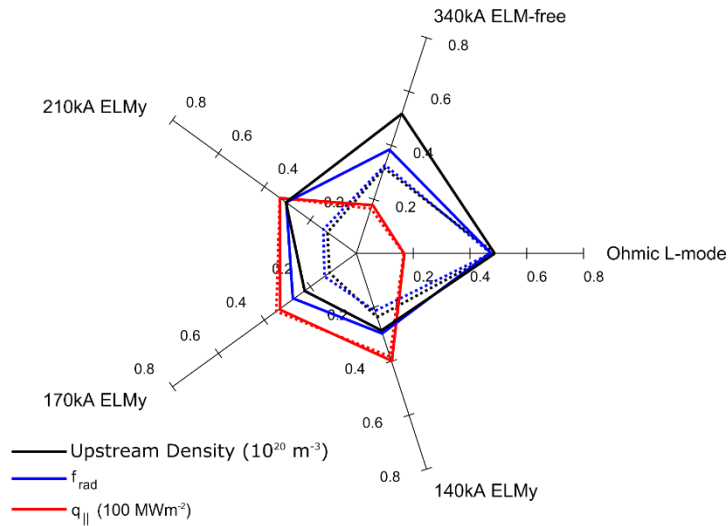
*Figure 5: Comparison of the H-mode experiments, in terms of the upstream density (black), frad (blue) and upstream parallel heat flux (red), in the ELMy and ELM-free scenarios studied, in the presence (solid) and absence (dashed) of additional fuelling and seeding to promote divertor detachment. For comparison, these quantites are plotted for the ohmic L-mode shot 52065 at the detachment threshold [Harrison2017,Verhaegh2017]*
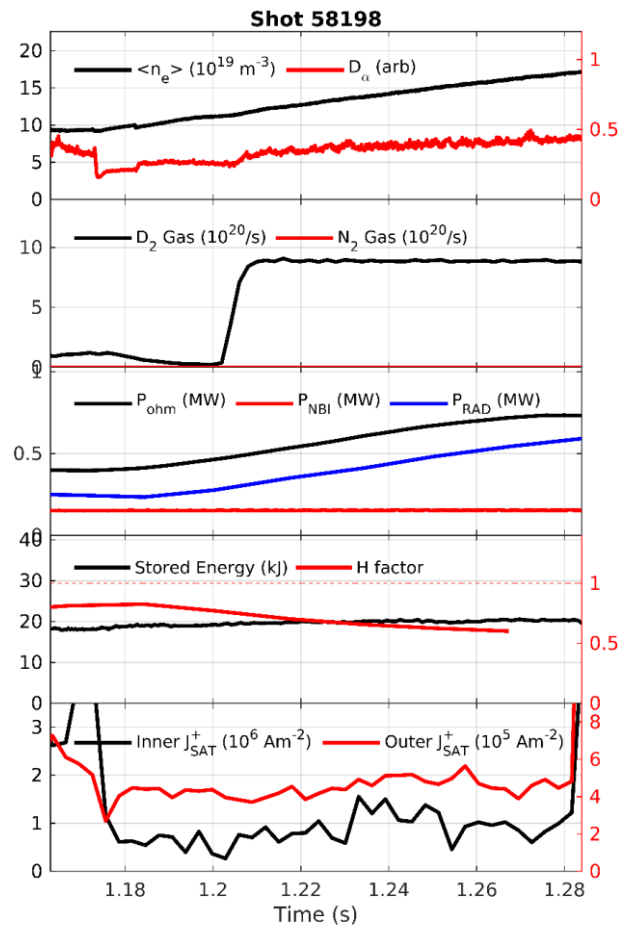


*Figure 6: Overview of a typical ELM-free H-mode shot, showing the evolution of the line average density, divertor Dα emission, gas fuelling and seeding rates, plasma power sources and sinks, stored energy and confinement quality and the total particle flux to the inner and outer divertors.*
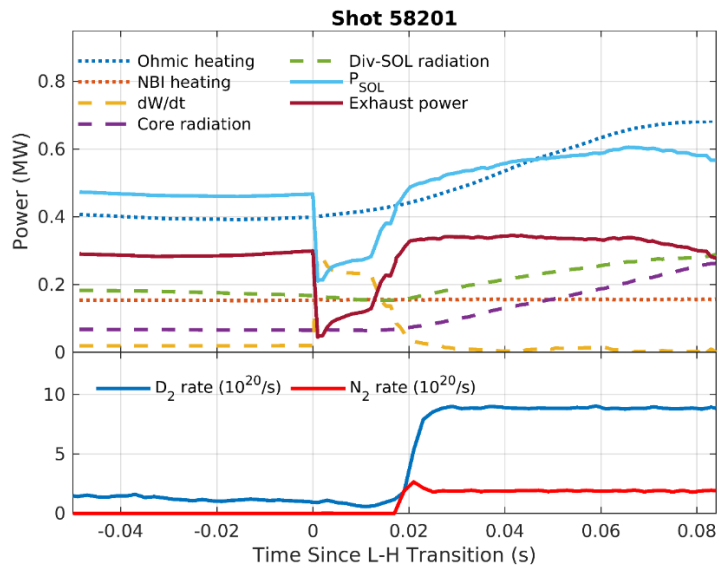
*Figure 7: Global power balance in a nitrogen seeded ELM-free shot. In the upper plot, the power sources are indicated as dotted lines and sinks as dashed lines. The power crossing the separtrix, $P_{SOL}$, and the exhaust power (i.e. $P_{SOL}$-power radiataed in the SOL and divertor) are plotted in solid lines. The gas fuelling and seeding rates are shown in the lower plot.*
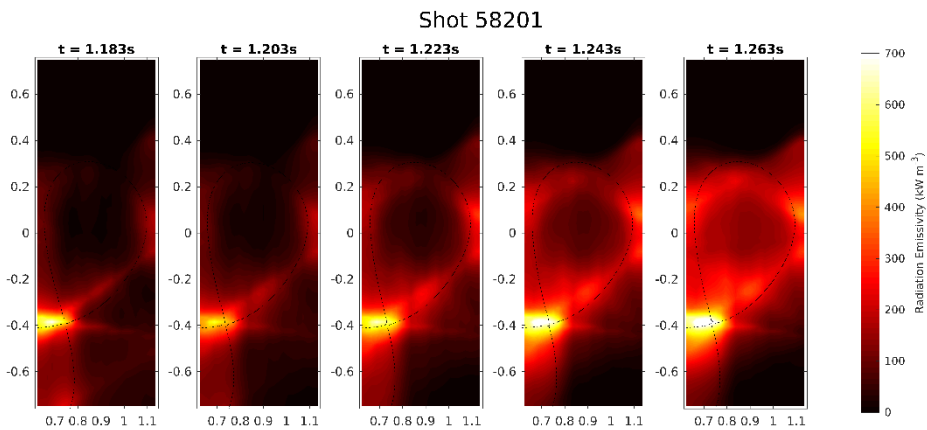


*Figure 8: Radiation emissivity profiles estimated from tomographically inverted foil bolometer data taken from a nitrogen seeded ELM-free H-mode shot from the time following the L-H transition to just prior to a disruption.*
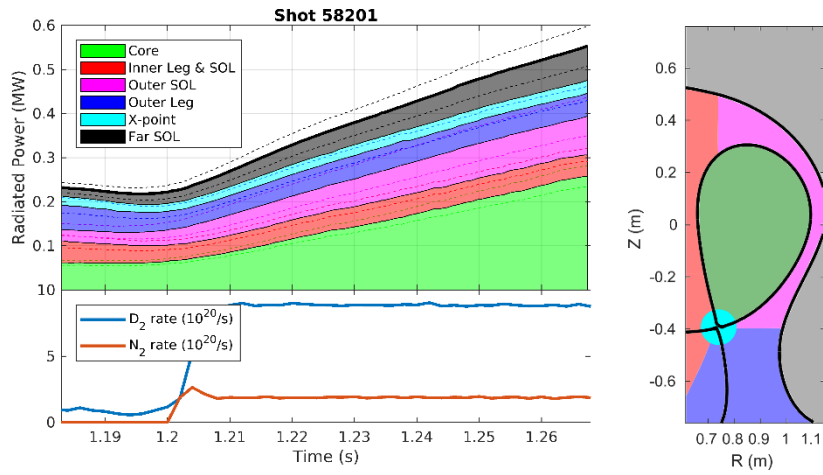
Figure 9: (Left) Breakdown of the radiated power measured by the foil bolometers in terms of its origin within the plasma for a nitrogen seeded ELM-free H-mode shot. The dashed lines indicate uncertainties in each measurement, estimated by varying the regularization parameter used in the tomographic reconstructions. (Right) description of the plasma regions used in the left plot.
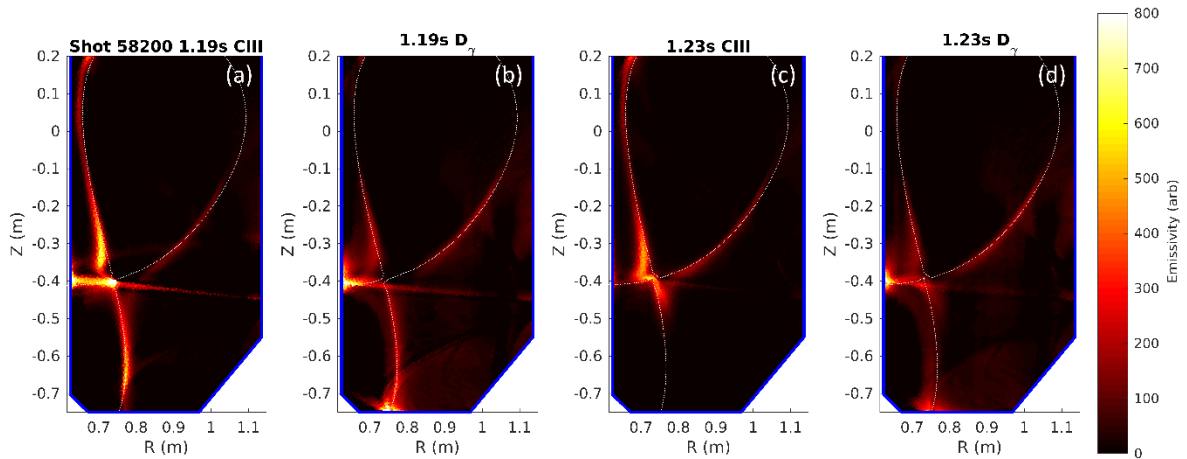


Figure 10: Inverted 2D emissivity profiles of impurity emission (labelled CIII) and deuterium Balmer $\gamma$ emission at the start (a,b) and end (c,d) of the ELM-free H-mode phase with impurity seeding to promote cooling in the divertor.
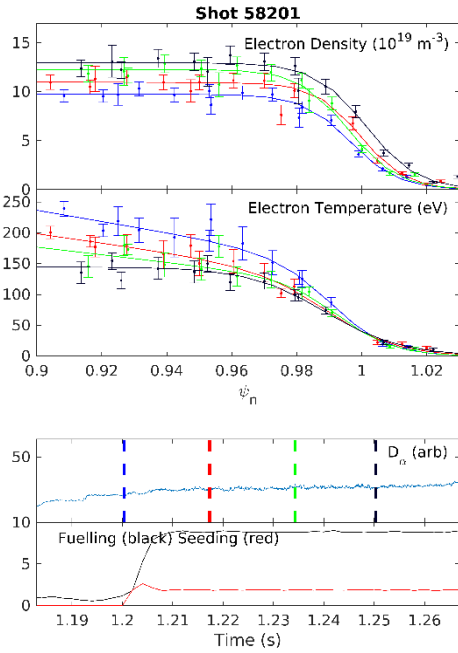
*Figure 11: Fitted Thomson scattering profiles during the fuelling and nitrogen seeding phase of an ELM-free H-mode shot.*
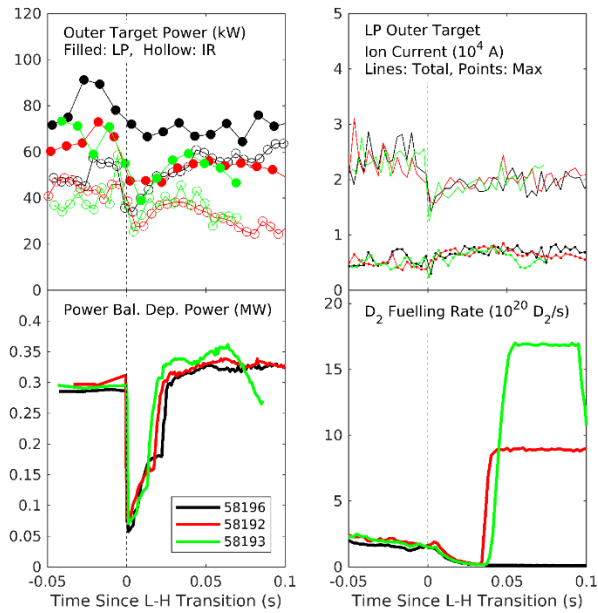


*Figure 12: Evolution of the outer divertor power and particle loads in shots with varying fuelling from the lower divertor, from no fuelling (black), an intermediate fuelling rate (red) and highest rate (green). (upper left) total power incident to the outer divertor estimated with Langmuir probes (filled points) and IR thermography (hollow points), (upper right) total and maximum ion current to the outer divertor, (lower left) power incident to the outer divertor estimated from power balance, (lower right) divertor fuelling rate.*
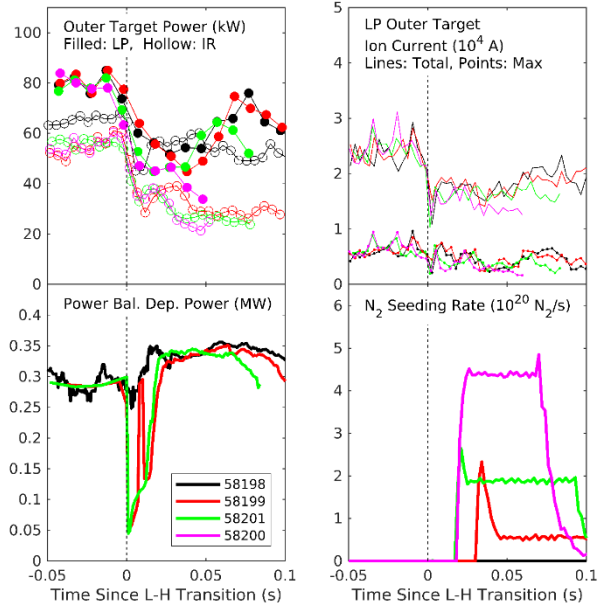
*Figure 13: Evolution of the outer divertor power and particle loads with a combination of fuelling and increasing nitrogen seeding. The quantities plotted are the same as in the previous figure.*
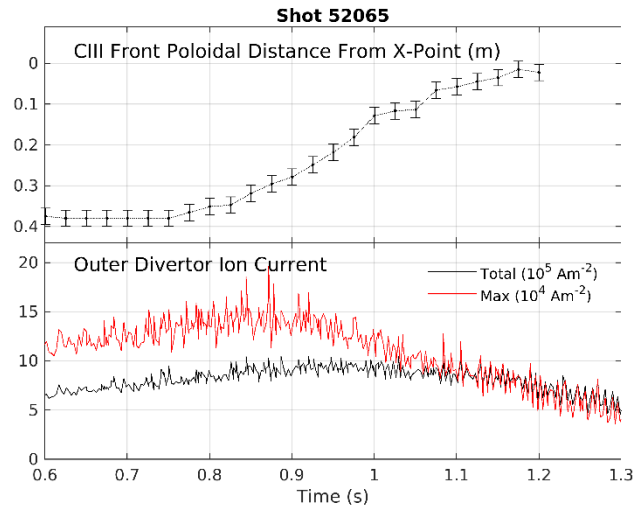


*Figure 14: Time evolution of the CIII emission front location along the outer leg (top) and the total and peak ion current to the outer divertor (bottom) during an L-mode ohmically heated density ramp experiment [Harrison2017]. A reduction in the ion current, characteristic of the onset of detachment, occurs when the front is approximately half way between the target and the X-point.*
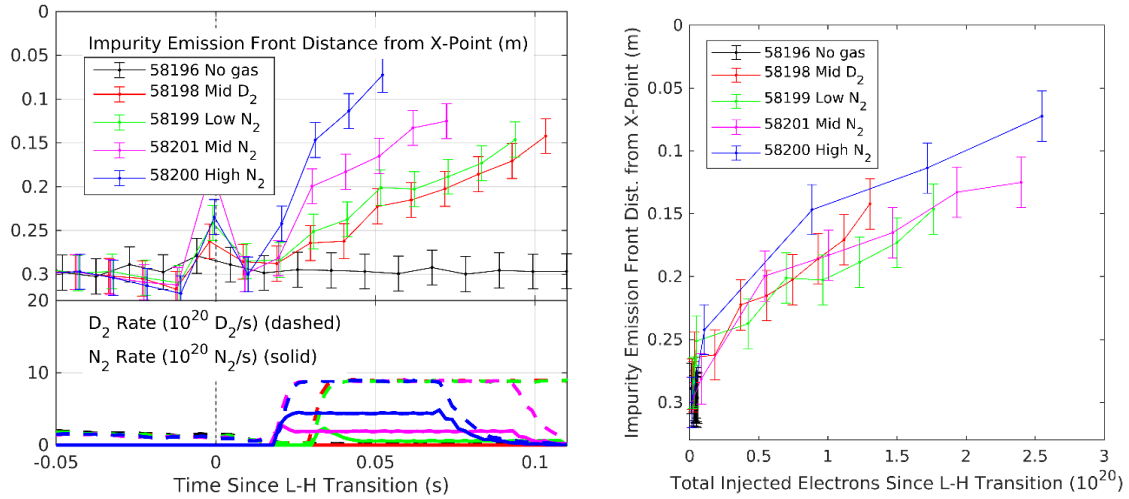
*Figure 15: Movement of the impurity emission front along the outer leg in shots with fuelling and increasing nitrogen seeding in time (left) and number of injected electrons since the L-H transition (right).*
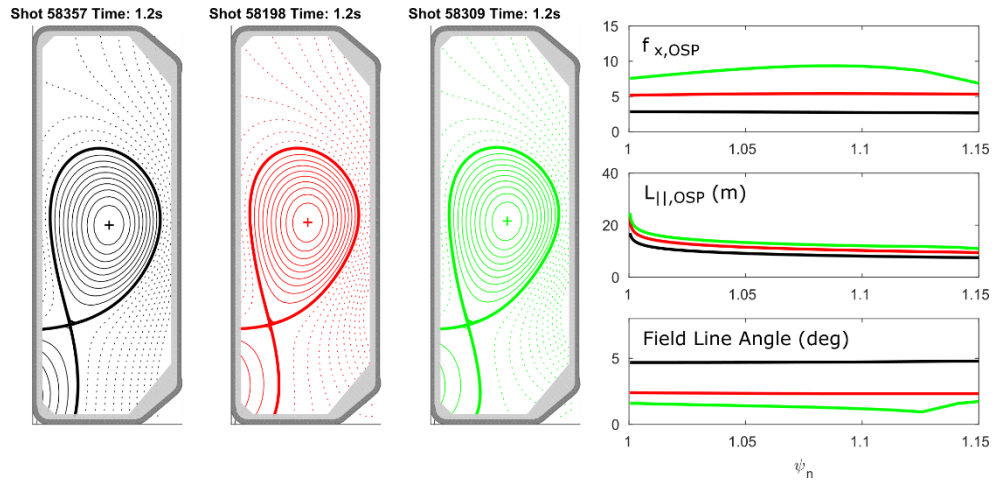


*Figure 16: (left) equilibria of the shots in the poloidal flux expansion scan, (right) from top to bottom, poloidal flux expansion, parallel connection length and field line incidence angle profiles of the outer divertor.*
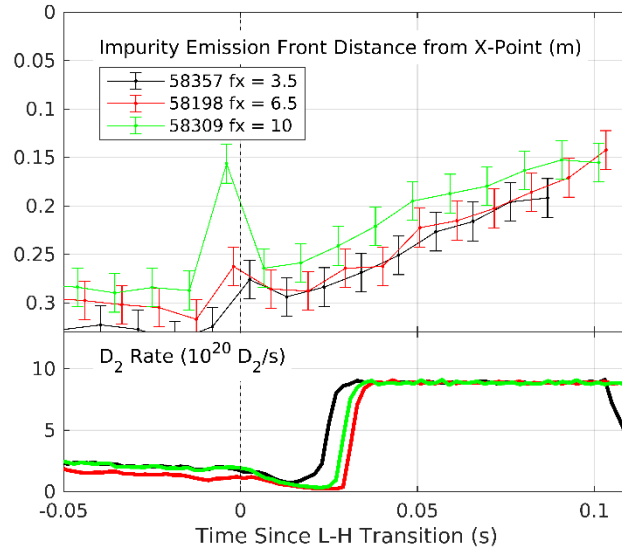
*Figure 17: Evolution of the impurity emission front location in fuelled ELM-free H-mode shots with different outer divertor poloidal flux expansion.*
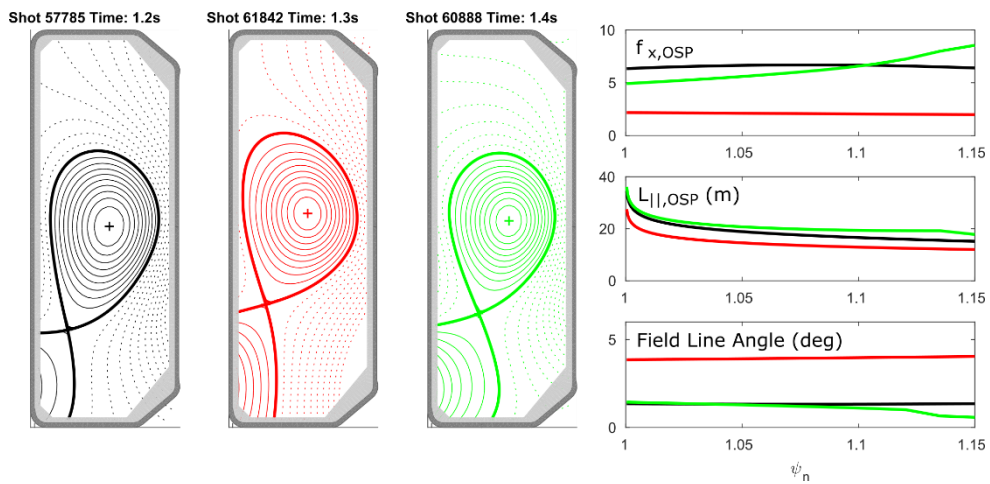


*Figure 18: Representative equilibria of the 210kA (left), 170kA (centre) and 140kA (right) ELMy H-mode scenarios.*
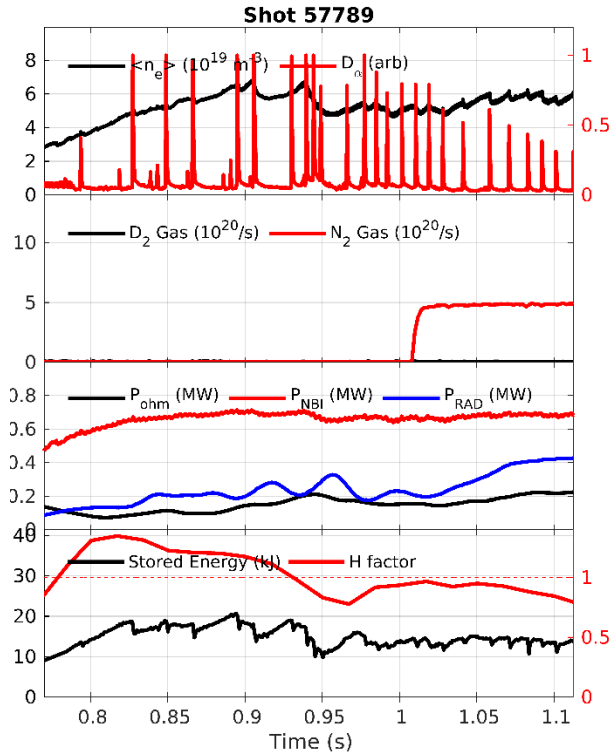
*Figure 19: Overview of a nitrogen seeded ELMy H-mode shot, showing (from top to bottom) the evolution of the line average density, divertor $D_\alpha$ emission, gas fuelling and seeding rates, plasma power sources and sinks, stored energy and confinement quality.*
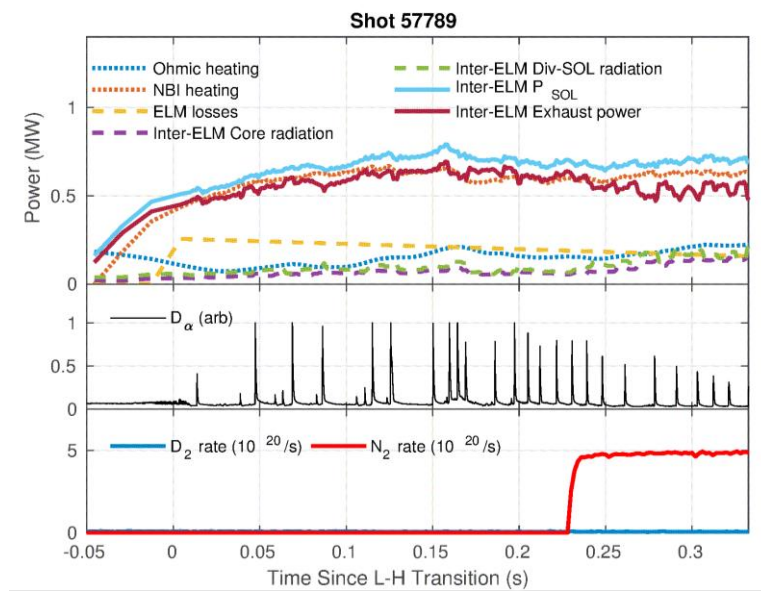


*Figure 20: Global power balance in a nitrogen ELMy H-mode shot.*
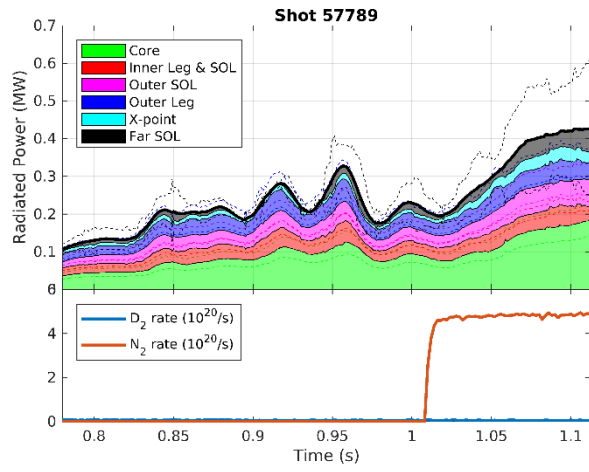
*Figure 21: Breakdown of the inter-ELM radiated power measured by the foil bolometers in terms of its origin within the plasma for a nitrogen seeded ELMy H-mode shot.  The dashed  lines indicate uncertainties in each measurement.*
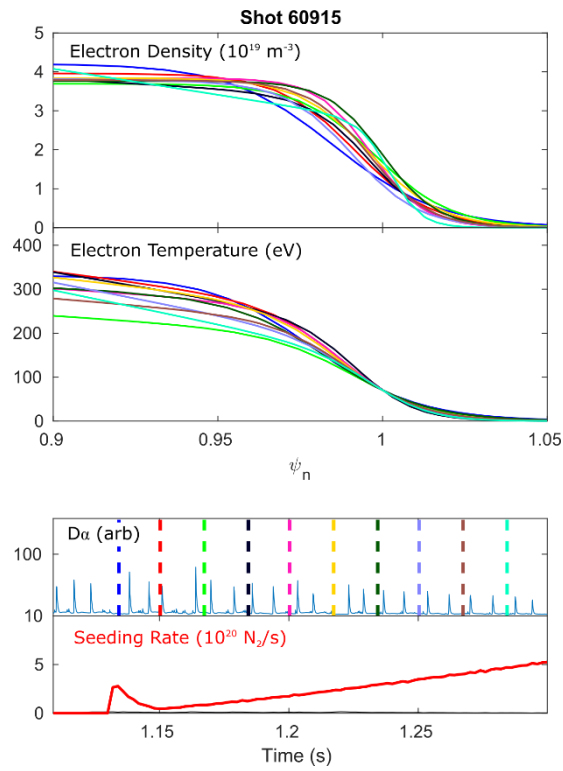


*Figure 22: Evolution of pedestal temperature and density profiles during a nitrogen seeding ramp experiment.  For clarity, only the fitted profiles are shown.*
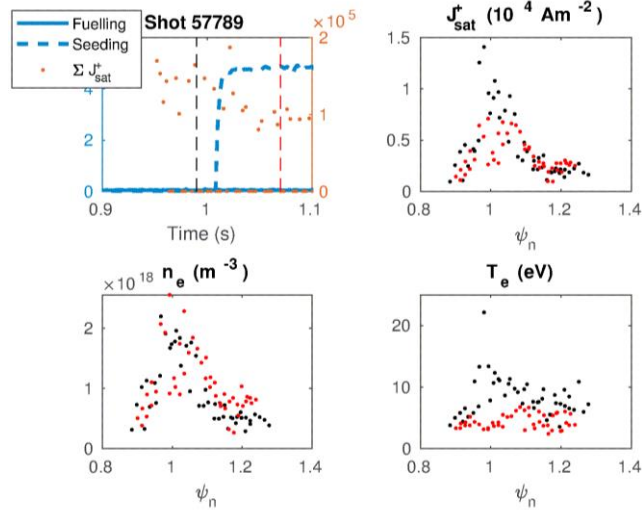
*Figure 23: Summary of Langmuir probe measurements. (upper left) time traces of the nitrogen seeding rate and total ion flux to the outer divertor (upper right, lower left, lower right) Ion saturation current density, electron density and electron temperature profiles measured at the times indicated by dashed lines in the upper right plot.*
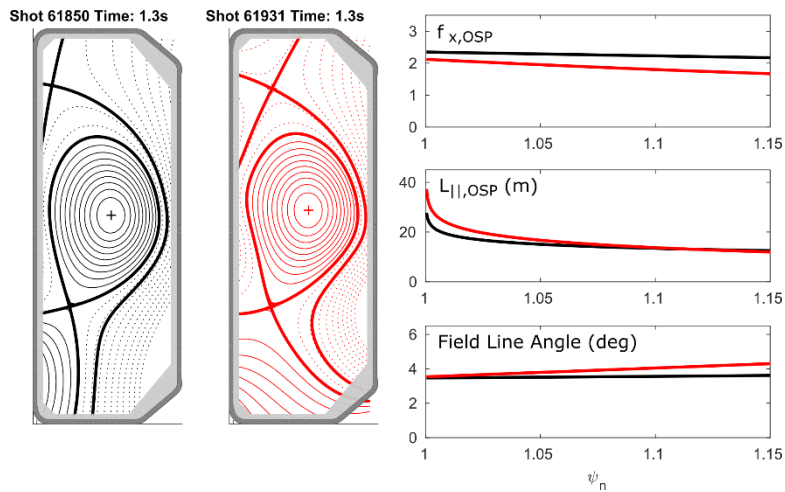


*Figure 24: Equilibria from experiments to study the effect of varying the total flux expansion out the outer divertor by varying the major radius from 0.75m to 1.03m.*
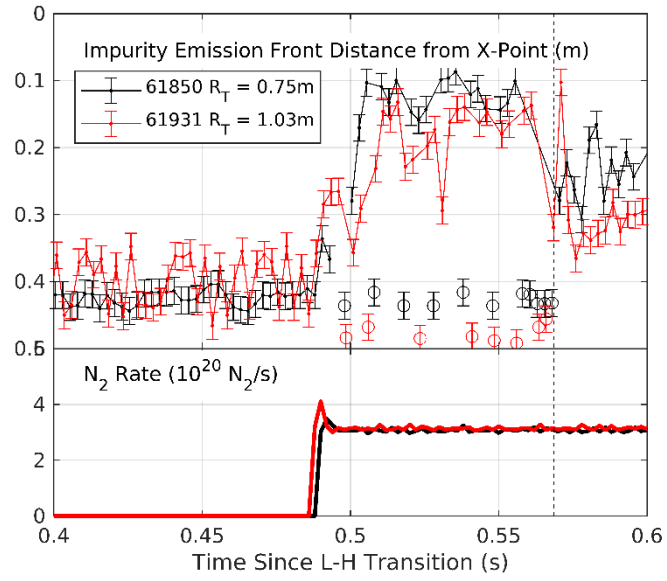
*Figure 25: Outer leg impurity front location between ELMs in shots with different strike point major radius. Measurements taken during ELMs are shown as hollow points. A back-transition to L-mode ~0.57s after the L-H transition is indicated by a dashed line.*